THE ASTROPHYSICAL JOURNAL, 425:343–347, 1994 April 10

SOLAR CORONAL TEMPERATURE DIAGNOSTICS USING EMISSION LINES FROM MULTIPLE STAGES OF IONIZATION OF IRON

JEFFREY W. BROSIUS,[1] JOSEPH M. DAVILA, ROGER J. THOMAS, AND WILLIAM T. THOMPSON[2]
Laboratory for Astronomy and Solar Physics, Code 682, NASA/Goddard Space Flight Center, Greenbelt, MD 20771[3]
Received 1993 August 2; accepted 1993 October 14

ABSTRACT

We obtained spatially resolved extreme-ultraviolet (EUV) spectra of AR 6615 on 1991 May 7 with NASA/Goddard Space Flight Center's Solar EUV Rocket Telescope and Spectrograph (SERTS). Included are emission lines from four different stages of ionization of iron: Fe^{+15} λ335 Å, Fe^{+14} λ327 Å, Fe^{+13} λ334 Å, and Fe^{+12} λ348 Å. Using intensity ratios from among these lines, we have calculated the active region coronal temperature along the SERTS slit. Temperatures derived from line ratios which incorporate adjacent stages of ionization are most sensitive to measurement uncertainties and yield the largest scatter. Temperatures derived from line ratios which incorporate nonadjacent stages of ionization are less sensitive to measurement uncertainties and yield little scatter. The active region temperature derived from these latter ratios has an average value of 2.54×10^6 K, with a standard deviation $\sim 0.12 \times 10^6$ K, and shows no significant variation with position along the slit.

Subject headings: atomic processes — Sun: corona — Sun: UV radiation

1. INTRODUCTION

The measurement of solar coronal plasma parameters such as temperature, emission measure, and density is essential for understandng basic processes occurring on the Sun. For example, well-determined values for the temperature and emission measure are necessary for a meaningful comparison with coordinated microwave observations to yield the coronal magnetic field (e.g., Brosius et al. 1993; Schmelz et al. 1992, and references therein). This ultimately provides insight into coronal processes such as heating and flare energy storage.

During the *Solar Maximum Mission* era, coronal temperatures were obtained by comparing the measured intensity ratio of emission lines originating from ions of different elements with their corresponding temperature-dependent theoretical curves. This technique works reasonably well (e.g., Brosius et al. 1992; Nitta et al. 1991) but can be hampered by uncertainties in the coronal elemental abundances (Meyer 1993; Falconer, Davila, & Thomas 1993; Saba & Strong 1993; Schmelz, Strong, & Lemen 1993; Widing & Feldman 1993; Feldman 1992). This problem is eliminated by using emission lines from successive stages of ionization of the same element and is the topic of the present study. Since the *SOHO* spacecraft will also be capable of observing the Sun in the same emission lines considered here, this analysis can be viewed as a case study of *SOHO* capabilities.

We obtained spectra of AR 6615 on 1991 May 7 with NASA/Goddard Space Flight Center's Solar EUV Rocket Telescope and Spectrograph (SERTS). In § 2 we describe the observations, in § 3 we describe the analysis of the data, in § 4 we discuss the results of the analysis, and in § 5 we emphasize our conclusions from this study.

[1] Also, Hughes STX Corporation, 4400 Forbes Boulevard, Lanham, MD 20706.
[2] Also, Applied Research Corporation, 8201 Corporate Drive, Landover, MD 20785.
[3] Postal address.

2. OBSERVATIONS

The SERTS imaging spectrograph is described by Neupert et al. (1992). The spectrograph entrance aperture was designed so that both spectra and spectroheliograms can be obtained simultaneously: spectra are obtained along a narrow 4.'9 long slit connecting two rectangular lobes within which the spectroheliograms are imaged. The upper lobe covers a 4.'8 × 8.'2 area on the Sun, and the lower one covers a 4.'8 × 7.'6 area. The spatial resolution is $\sim 7''$, and the spectral resolution is < 75 mÅ. By adjusting the pointing of the instrument during its flight, both images and spectra can be obtained for the same portion of the Sun.

SERTS was launched on a Terrier-boosted Black Brant rocket from White Sands, New Mexico at 1805 UT on 1991 May 7. It reached a maximum altitude of 327 km, and acquired spectrographic data from 1806 to 1813 UT. This was the first flight of a multilayer coated diffraction grating (Davila et al. 1992; Keski-Kuha, Thomas, & Davila 1992; Thomas et al. 1991). The instrument performed well, and we obtained spectra and spectroheliograms in the spectral range of 235 to 450 Å. In the first of two pointing positions, we obtained spectroheliograms of AR 6615 (S10,W30, in the upper lobe) and off-limb areas (in the lower lobe) and spectra of the quiet sun between them. In the second pointing position, we obtained spectroheliograms of plage (N11,W10, in the upper lobe) and AR 6608 (S22,W63, in the lower lobe) and spectra of AR 6615. We also obtained simultaneous ground-based observations of the active regions and the plage with the NASA/National Solar Observatory spectromagnetograph (Jones et al. 1992) and with the Very Large Array. Active region vector magnetograms were obtained with the University of Hawaii's Stokes Polarimeter, and active region Hα spectroheliograms were obtained with the multichannel subtractive double pass (MSDP) spectrograph on the Canary Islands (Schmieder et al. 1992). Detailed analysis of the plage observations is discussed by Brosius et al. (1993). The active regions, for which the largest amount of data is available, remain to be analyzed.

For each SERTS pointing position we obtained images at four different exposure times to ensure the availability of optimally exposed images and spectra for emission lines covering a wide range of intensities. The images were recorded on Eastman Kodak 101-07 EUV-sensitive photographic film and digitized with a Perkin-Elmer microdensitometer. We estimate that relative line intensities are accurate to better than 20% at wavelengths above 300 Å (perhaps somewhat worse at wavelengths below 300 Å) and that the absolute photometric scale is accurate to better than a factor of 2. Details of the SERTS calibration procedures are given by Thomas & Neupert (1994), Brosius et al. (1993), and Thompson et al. (1993). In this paper we concentrate only on spectra from the slit which grazed AR 6615.

The SERTS spectroheliograms and slit spectra were coaligned with the ground-based observations by matching features common to both the SERTS He II 304 Å image and the Kitt Peak He I 10830 Å image. Discussion of the coalignment procedure can be found in Brosius et al. (1993). The formal uncertainty in the coalignment is $\sim 10''$. Figure 1 shows the pointing of the SERTS instrument on the full-disk Kitt Peak magnetogram, and marks the portion of the slit which is used in our analysis. Integrated intensities of 12 individual pixels along the slit are given in Table 1. The first entry in the table corresponds to the right-hand (west) side of the slit segment seen in Figure 1. There are actually 14 pixels between the two markers indicated in Figure 1, but two of the pixels are contaminated. We have used three different exposures to obtain the intensities in Table 1, so as to always remain within the linear portion of the film's D-log E relation. The intensities are in ergs cm^{-2} s^{-1} sr^{-1}.

TABLE 1

INTEGRATED INTENSITIES OF SLIT EMISSION LINES IN ergs cm^{-2} s^{-1} sr^{-1}

Pixel	Fe^{+15}(335)	Fe^{+14}(327)	Fe^{+13}(334)	Fe^{+12}(348)
1	2.09×10^4	1.91×10^2	9.56×10^2	1.81×10^2
2	2.25×10^4	2.50×10^2	1.15×10^3	5.43×10^2
3	2.14×10^4	1.90×10^2	1.68×10^3	4.11×10^2
4	2.18×10^4	1.65×10^2	1.40×10^3	3.87×10^2
5	1.76×10^4	1.65×10^2	1.68×10^3	4.24×10^2
6	1.87×10^4	2.09×10^2	1.31×10^3	3.48×10^2
7	2.00×10^4	2.82×10^2	1.34×10^3	1.84×10^2
8	...	...	...	...
9	...	...	...	...
10	2.15×10^4	2.20×10^2	1.34×10^3	2.58×10^2
11	1.90×10^4	3.17×10^2	1.28×10^3	3.50×10^2
12	2.02×10^4	2.03×10^2	1.20×10^3	2.76×10^2
13	2.01×10^4	2.27×10^2	1.11×10^3	3.36×10^2
14	2.06×10^4	2.41×10^2	1.12×10^3	2.16×10^2
AVG	2.04×10^4	2.22×10^2	1.30×10^3	3.26×10^2

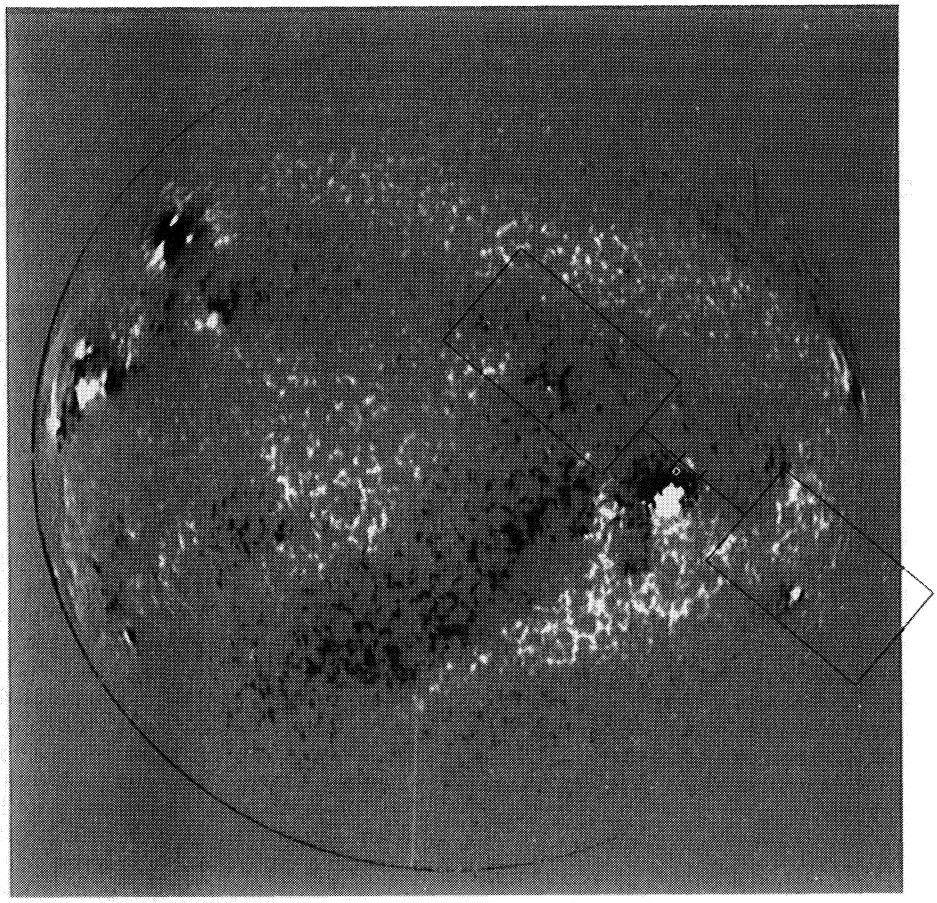

FIG. 1.—Pointing of the SERTS imaging spectrograph during the flight of 1991 May 7. The lobes and slit are shown on the full-disk Kitt Peak magnetogram. In this pointing position the slit crossed the edge of AR 6615. The short lines perpendicular to the slit indicate the segment of the slit used in this analysis. The right-hand (west) side of this segment corresponds to the first pixel in the following plots. Solar north is at the top.

TABLE 2

ATOMIC PARAMETERS FOR THE EMISSION LINES USED IN THIS PAPER

Ion	λ (Å)	E_{gj} (10^{-11} ergs)	E_{jk} (10^{-11} ergs)	ω_g	Ω_{gj}	B_{jk}	References
Fe^{+15}	335.41	5.923	5.923	2	2.47	1.0	1, 2
Fe^{+14}	327.06	11.12	6.074	1	0.079	0.426	3
Fe^{+13}	334.17	5.944	5.944	2	0.693	0.97	4
Fe^{+12}	348.18	5.705	5.705	1	0.381	0.79	5

REFERENCES.—(1) Flower & Nussbaumer 1975; (2) Blaha & Davis 1978; (3) Bhatia & Kastner 1980; (4) Dufton & Kingston 1991; (5) Neupert & Kastner 1983 (and references therein).

3. ANALYSIS

The rate of emission per unit volume for a spectral line which emits by radiative decay following collisional excitation is given by

$$P_{jk} = N_i N_e C_{gj} B_{jk} E_{jk} \quad (1)$$

(e.g., Stern, Wang, & Bowyer 1978; Landini & Monsignori-Fossi 1990), where g corresponds to the ground state, j corresponds to the excited state, and k corresponds to the final state; N_i is the number density of appropriate ions, N_e is the number density of electrons, B_{jk} is the branching ratio, E_{jk} is the energy of the emitted photon, and C_{gj} is the collisional excitation rate

$$C_{gj} = 8.63 \times 10^{-6}(\Omega_{gj}/\omega_g T^{1/2}) \exp(-E_{gj}/kT), \quad (2)$$

in which ω_g is the statistical weight of the ground state, Ω_{gj} is the collision strength from the ground level, T is the temperature, k is Boltzmann's constant, and E_{gj} is the energy of the transition from the ground state to the excited state. Equation (1) can be rewritten as

$$P_{jk} = (N_i/N_E)(N_E/N_H) N_H N_e C_{gj} B_{jk} E_{jk}, \quad (3)$$

where N_i/N_E is the fraction of particles of the given element which are in the appropriate stage of ionization, N_E/N_H is the element abundance with respect to hydrogen, and N_H is the hydrogen number density.

The intensity ratio of two lines formed from different stages of ionization (the ath and the bth) of the same element follows:

$$\frac{I_a}{I_b} = \frac{(N_i/N_E)_a E^a_{jk} B^a_{jk} \Omega^a_{gj} \omega^b_g}{(N_i/N_E)_b E^b_{jk} B^b_{jk} \Omega^b_{gj} \omega^a_g} \exp[(E^b_{gj} - E^a_{gj})/kT]. \quad (4)$$

Since the emission lines that we use are close together in wavelength, the temperature sensitivity of this relation is dominated by the temperature dependence of the ionization fractions for the two different stages of ionization.

We adopt the ionization fraction calculations of Arnaud & Raymond (1992) for use in our calculations of the theoretical relationship between line intensity ratio and temperature. The Fe^{+15} fraction peaks at log $T = 6.4$, while that of Fe^{+14}, Fe^{+13}, and Fe^{+12} peaks at log $T = 6.3$, 6.3, and 6.2, respectively. Atomic parameters for the emission lines used in this paper are given in Table 2. The branching ratios are determined from the transition probabilities to all states out of the excited state as tabulated by Fuhr, Martin, & Wiese (1988). Combining all of the relevant quantities, we find that the temperature can be determined from the line ratio R ($= I_a/I_b$ of eq. 4) by the expression

$$\log T = \alpha + \beta R^{\gamma}. \quad (5)$$

Values of α, β, and γ are listed in Table 3 for the line intensity ratios used in this paper.

We assume in these calculations that the exciting transitions are out of the ground level only and that the populations of all levels but the ground level are negligible (i.e., we assume a low-density plasma). For comparison, however, we have repeated our calculations using line emissivities provided by Monsignori-Fossi (1992). These emissivities, as yet unpublished, incorporate many-level atoms with density-dependent population levels and include the ionization fraction calculations of Arnaud & Raymond (1992). They yield the same dependence of temperature upon line intensity ratio as in equation (5). The corresponding parameters are listed in Table 3 (α_1, β_1, γ_1) for an assumed electron density of 10^9 cm^{-3}. The temperatures derived using these calculations are systematically lower than, but similar in value to, those derived using the low-density calculations.

4. RESULTS

In Figure 2 we plot the temperature calculated for all of the line ratios used for each of the individual pixels along the slit. Because we have used six different line intensity ratios, there are six symbols marked for each pixel. The solid line indicates the average of all the temperature values (log $T = 6.412$, or $T = 2.58 \times 10^6$ K), and the dotted lines indicate 1 σ from this average ($\sigma = 0.041$, or $\Delta T = {}^{+0.26}_{-0.23} \times 10^6$ K). Notice that, although there is some scatter about the average, there is a

TABLE 3

PARAMETERS USED IN EQUATION (5)[a]

Ratio	α	β	γ	α_1	β_1	γ_1
$Fe^{+15}(335)/Fe^{+14}(327)$	5.787	0.252	0.216	5.734	0.300	0.187
$Fe^{+15}(335)/Fe^{+13}(334)$	5.731	0.522	0.0923	5.733	0.503	0.0931
$Fe^{+15}(335)/Fe^{+12}(348)$	5.688	0.567	0.0594	5.757	0.479	0.0660
$Fe^{+14}(327)/Fe^{+13}(334)$	5.671	0.915	0.159	5.732	0.840	0.185
$Fe^{+14}(327)/Fe^{+12}(348)$	5.629	0.789	0.0804	5.586	0.803	0.0792
$Fe^{+13}(334)/Fe^{+12}(348)$	5.571	0.688	0.161	5.544	0.682	0.159

[a] Subscripted parameters are derived from line emissivities tabulated by Monsignori-Fossi 1992, for an electron density of 10^9 cm^{-3}.

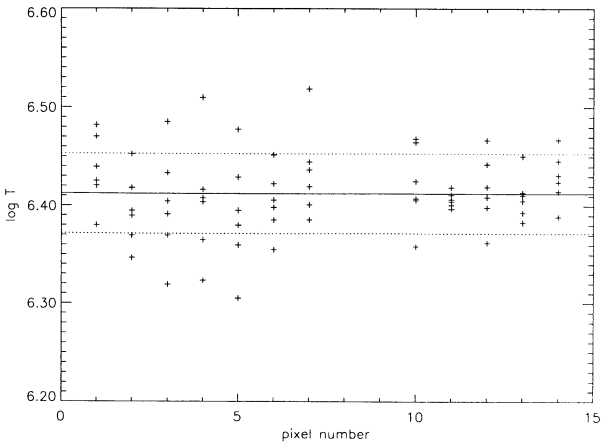

FIG. 2.—Temperature calculated using six different line intensity ratios for each of 12 pixels along the SERTS slit. The solid horizontal line shows the average of all the measurements, and the dotted horizontal lines show 1 σ from the average.

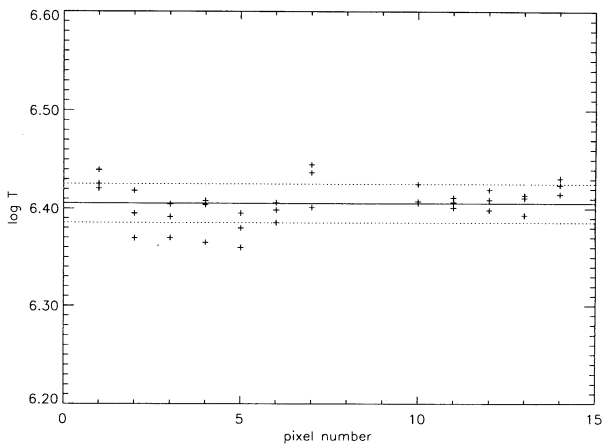

FIG. 3.—Temperature calculated using three different line intensity ratios involving nonadjacent stages of ionization of iron for each of 12 pixels along the SERTS slit. The solid horizontal line shows the average of all the measurements, and the dotted horizontal lines show 1 σ from the average.

clear tendency for the temperature values to cluster around log $T = 6.41$. There are no calculated temperatures as low as log $T = 6.2$ (even though one of the lines in our sample has its peak ionization fraction at this temperature), and there is very little clustering of temperature values around log $T = 6.3$ (even though two of the lines in our sample have their peak ionization fraction at this temperature).

The scatter in Figure 2 can be understood by recognizing that some of the line intensity ratios that we have used are significantly more sensitive to measurement uncertainties and atomic parameter uncertainties than others. Indeed, the larger the theoretical variation of a given line intensity ratio over a given temperature range, the less sensitive that line ratio is to the uncertainties. The ratio $Fe^{+15}(335)/Fe^{+12}(348)$ has the largest variation of any of our line ratios over any given temperature range, making it our ratio which is least sensitive to measurement uncertainties. For example, assuming a total uncertainty of 20% in the line intensity ratios (the estimated uncertainty in the relative flux calibration described above), and using the average intensities listed in Table 1, we find that log T has an uncertainty of $(^{+0.007}_{-0.010})$ when calculated using $Fe^{+15}(335)/Fe^{+12}(348)$, $(^{+0.011}_{-0.014})$ using $Fe^{+15}(335)/Fe^{+13}(334)$, $(^{+0.012}_{-0.013})$ using $Fe^{+14}(327)/Fe^{+12}(348)$, $(^{+0.020}_{-0.024})$ using $Fe^{+14}(327)/Fe^{+13}(334)$, $(^{+0.026}_{-0.030})$ using $Fe^{+13}(334)/Fe^{+12}(348)$, and $(^{+0.027}_{-0.032})$ using $Fe^{+15}(335)/Fe^{+14}(327)$. Notice that the line intensity ratios which yield the largest uncertainties on the calculated temperatures are those involving adjacent stages of ionization of iron. This is because the differences in ionization fraction are the smallest for adjacent stages of ionization. It is these line ratios which cause the largest scatter in the calculated temperatures plotted in Figure 2.

In Figure 3 we plot the temperature calculated for the three line ratios which do not involve adjacent stages of ionization for each of the individual pixels along the slit. Emission lines from all four stages of ionization of iron are included in these three ratios. The average temperature (log $T = 6.405$, or $T = 2.54 \times 10^6$ K) is nearly the same as in Figure 2, but there is considerably less scatter in Figure 3 ($\sigma = 0.020$, or $\Delta T = {}^{+0.12}_{-0.11} \times 10^6$ K). For comparison, we calculate the average temperature and the standard deviation for the three line ratios which involve only adjacent stages of ionization, and we obtain log $T = 6.420$ ($T = 2.63 \times 10^6$ K) and $\sigma = 0.053$ ($\Delta T = {}^{+0.34}_{-0.30} \times 10^6$ K).

In Figure 4*a* we plot the temperature calculated at each pixel using the ratio $Fe^{+15}(335)/Fe^{+12}(348)$. The vertical line through each asterisk indicates the uncertainty on the calculated temperature assuming a 20% uncertainty in the line intensity ratio. The solid horizontal line indicates the average, and the dotted lines indicate 1 σ from the average. Figure 4*b* shows the temperature calculated using $Fe^{+15}(335)/Fe^{+13}(334)$, and Figure 4*c* $Fe^{+14}(327)/Fe^{+12}(348)$. Because all of the individual temperature measurements lie so close to their respective average values, none of the line ratios indicate any significant temperature variations along the portion of the slit used in this analysis. Furthermore, the slit-averaged temperatures obtained for each of the line ratios used in Figure 4, log $T = 6.415$, 6.405, and 6.396, respectively, are within the uncertainties listed above from each other. Thus we conclude that the coronal temperature along the portion of the SERTS slit which grazed AR 6615 remained fairly constant at its average value of log $T = 6.405$, or $T = 2.54 \times 10^6$ K. This value was determined by using three independent line intensity ratios, all relatively insensitive to measurement uncertainties, encompassing emission lines from four different stages of ionization of iron.

For comparison, using the Monsignori-Fossi (1992) calculations, we find that the average temperature value derived combining all six line intensity ratios is log $T = 6.385$ ($T = 2.43 \times 10^6$ K), and that the standard deviation from this average is $\sigma = 0.040$ ($\Delta T = {}^{+0.23}_{-0.22} \times 10^6$ K). Similarly, the average temperature for the line ratios which incorporate only nonadjacent stages of ionization is log $T = 6.380$ ($T = 2.40 \times 10^6$ K), with $\sigma = 0.020$ ($\Delta T = {}^{+0.11}_{-0.11} \times 10^6$ K), while the average temperature for the line ratios which incorporate only adjacent stages of ionization is log $T = 6.391$ ($T = 2.46 \times 10^6$ K), with $\sigma = 0.052$ ($\Delta T = {}^{+0.31}_{-0.28} \times 10^6$ K). The slit-averaged temperatures for the line ratios used in Figure 4*a*–4*c* are, respectively, log $T = 6.388$, log $T = 6.384$, and log $T = 6.367$. These are systematically lower than the corresponding values obtained using the low-density plasma results but support our conclusions drawn from the latter.

5. CONCLUSIONS

We have derived the coronal temperature using six different emission line intensity ratios along the portion of the SERTS

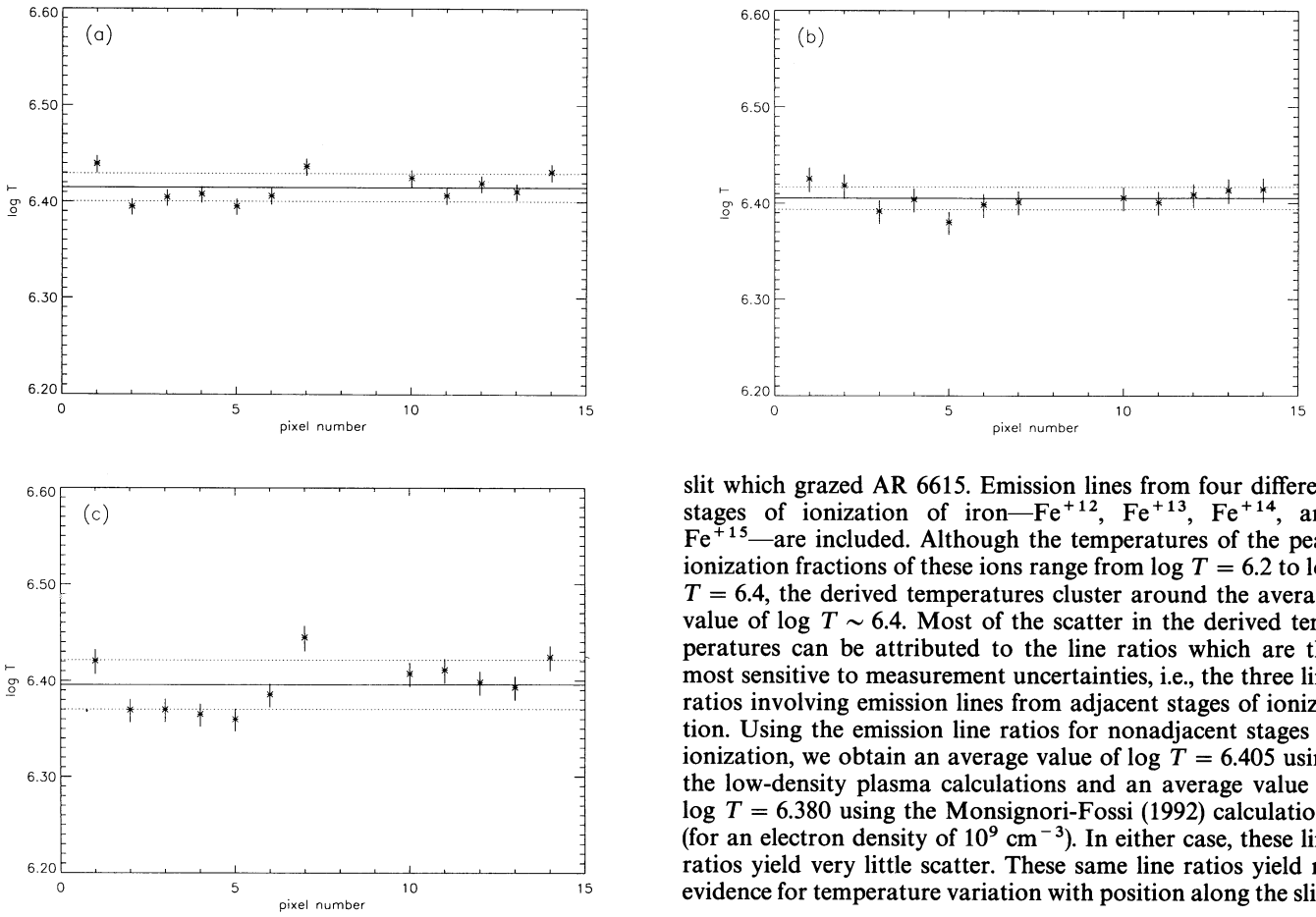

FIG. 4.—The temperature and its associated uncertainty calculated for each pixel along the slit using the intensity ratio (*a*) $Fe^{+15}(335)/Fe^{+12}(348)$, (*b*) $Fe^{+15}(335)/Fe^{+13}(334)$, and (*c*) $Fe^{+14}(327)/Fe^{+12}(348)$. The solid horizontal lines indicate the average temperature for each ratio, and the dotted horizontal lines indicate the average $\pm 1\ \sigma$.

slit which grazed AR 6615. Emission lines from four different stages of ionization of iron—Fe^{+12}, Fe^{+13}, Fe^{+14}, and Fe^{+15}—are included. Although the temperatures of the peak ionization fractions of these ions range from log $T = 6.2$ to log $T = 6.4$, the derived temperatures cluster around the average value of log $T \sim 6.4$. Most of the scatter in the derived temperatures can be attributed to the line ratios which are the most sensitive to measurement uncertainties, i.e., the three line ratios involving emission lines from adjacent stages of ionization. Using the emission line ratios for nonadjacent stages of ionization, we obtain an average value of log $T = 6.405$ using the low-density plasma calculations and an average value of log $T = 6.380$ using the Monsignori-Fossi (1992) calculations (for an electron density of 10^9 cm^{-3}). In either case, these line ratios yield very little scatter. These same line ratios yield no evidence for temperature variation with position along the slit.

Research at GSFC was supported in part by NASA RTOPs 170-38-53 and 879-11-38. NSO/Kitt Peak data used here are produced cooperatively by NSF/NOAO, NASA/GSFC, and NOAA/SEL.

REFERENCES

Arnaud, M., & Raymond, J. 1992, ApJ, 398, 394
Bhatia, A. K., & Kastner, S. O. 1980, Sol. Phys., 65, 181
Blaha, M., & Davis, J. 1978, J. Quant. Spectrosc. Rad. Transf., 19, 227
Brosius, J. W., et al. 1993, ApJ, 411, 410
Brosius, J. W., Willson, R. F., Holman, G. D., & Schmelz, J. T. 1992, ApJ, 386, 347
Davila, J. M., Thomas, R. J., Thompson, W. T., Keski-Kuha, R. A. M., & Neupert, W. M. 1993, UV and X-Ray Spectroscopy of Laboratory and Astrophysical Plasma, ed. E. Silver, S. Kahn (Cambridge: Cambridge), 301
Dufton, P. L., & Kingston, A. E. 1991, Physica Scripta, 43, 386
Falconer, D. A., Davila, J. M., & Thomas, R. J. 1993, BAAS, 25, 1200
Feldman, U. 1992, Phys. Scripta, 46, 202
Flower, D. R., & Nussbaumer, H. 1975, A&A, 42, 265
Fuhr, J. R., Martin, G. A., & Wiese, W. L. 1988, J. Phys. Chem. Ref. Data, 17, 1
Jones, H. P., Duvall, T. L., Jr., Harvey, J. W., Mahaffey, C. T., Schwitters, J. D., & Simmons, J. E. 1992, Sol. Phys., 139, 211
Keski-Kuha, R. A. M., Thomas, R. J., & Davila, J. M. 1992, Proc. SPIE, 1546, 614
Landini, M., & Monsignori-Fossi, B. C. 1990, A&AS, 82, 229
Meyer, J.-P. 1993, Adv. Space Res., in press
Monsignori-Fossi, B. C. 1992, private communication
Neupert, W. M., Epstein, G. L., Thomas, R. J., & Thompson, W. T. 1992, Sol. Phys., 137, 87
Neupert, W. M., & Kastner, S. O. 1983, A&A, 128, 188
Nitta, N., et al. 1991, ApJ, 374, 374
Saba, J. L. R., & Strong, K. T. 1993, BAAS, 25, 1201
Schmelz, J. T., Holman, G. D., Brosius, J. W., & Gonzalez, R. D. 1992, ApJ, 399, 733
Schmelz, J. T., Strong, K. T., & Lemen, J. R. 1993, BAAS, 25, 1201
Schmieder, B., Mein, N., Golub, L., Davila, J. M., Brosius, J., & Thomas, R. 1992, in Proc. 1st *SOHO* Workshop (ESA SP-348), 257
Stern, R., Wang, E., & Bowyer, S. 1978, ApJS, 37, 195
Thomas, R. J., Keski-Kuha, R. A. M., Neupert, W. M., Condor, C. E., & Gum, J. S. 1991, Appl. Opt., 30, 2245
Thomas, R. J., & Neupert, W. M. 1994, ApJS, in press
Thompson, W. T., Neupert, W. M., Jordan, S. D., Jones, H. P., Thomas, R. J., & Schmeider, B. 1993, Sol. Phys., 147, 29
Widing, K. G., & Feldman, U. 1993, BAAS, 25, 1201